Supplementary Information:

Hybrid Surface-Phonon-Plasmon Polariton Modes in Graphene / Monolayer h-BN stacks

Victor W. Brar[1,2†], Min Seok Jang[3,†], Michelle Sherrott[1], Seyoon Kim[1], Josue J. Lopez[1], Laura B. Kim[1], Mansoo Choi[3,4], and Harry Atwater[1,2]

† These authors contributed equally.

1) Thomas J. Watson Laboratory of Applied Physics, California Institute of Technology, Pasadena, CA 91125

2) Kavli Nanoscience Institute, California Institute of Technology, Pasadena, CA91125

3) Global Frontier Center for Multiscale Energy Systems, Seoul National University, Seoul 151-747, Republic of Korea

4) Division of WCU Multiscale Mechanical Design, School of Mechanical and Aerospace Engineering, Seoul National University, Seoul 151-742

I. Electromagnetic Simulations

We solve classical electromagnetic equations by employing the finite element method in order to simulate the plasmon oscillation in graphene nanoresonators. The sheet conductivity of graphene $\sigma(\omega)$ is evaluated within the local phase approximation.[1]

$$\sigma(\omega) = \frac{2ie^2T}{\pi\hbar(\omega + i\Gamma)}\log\left[2\cosh\left(\frac{E_F}{2T}\right)\right] + \frac{e^2}{4\hbar}[H\left(\frac{\omega}{2}\right) + \frac{4i\omega}{\pi}\int_0^\infty d\eta \frac{H(\eta) - H\left(\frac{\omega}{2}\right)}{\omega^2 - 4\eta^2},$$

where

$$H(\eta) = \frac{\sinh(\eta/T)}{\cosh(E_F/T) + \cosh(\eta/T)}.$$

Here, the temperature T is set as 300K. The carrier scattering rate Γ takes into account scattering by impurities with the carrier mobility of 500cm^2/Vs, and by optical phonons estimated from theoretically obtained self-energy.[2, 3] The in-plane and out-of-plane relative permittivity of graphene are then separately assigned as ε=1+$i\sigma/\omega\delta$ and 1, respectively. The thickness of graphene(δ) and h-BN are both set as 0.34nm from the interlayer spacing of bulk hBN and graphite. An oscillator model is used to describe in-plane dielectric function of h-BN,

$$\epsilon_{\mathrm{BN}}(\omega) = \epsilon_\infty + \sum_i \frac{s_i^2}{\omega_i^2 - \omega^2 + i\omega\gamma_i}$$

where ϵ_∞= 4.95 is the optical dielectric constant.[4] The parameters for strong in-plane phonon mode at ω_1=1370cm^{-1} are determined by fitting the theoretical extinction spectra to the measured data as $s_1^2 = 3.9\times10^6$cm^{-2}, and γ_1 = 19cm^{-1} (Fig. S1). The complex dielectric function of SiO2 is adopted from Palik.[5]

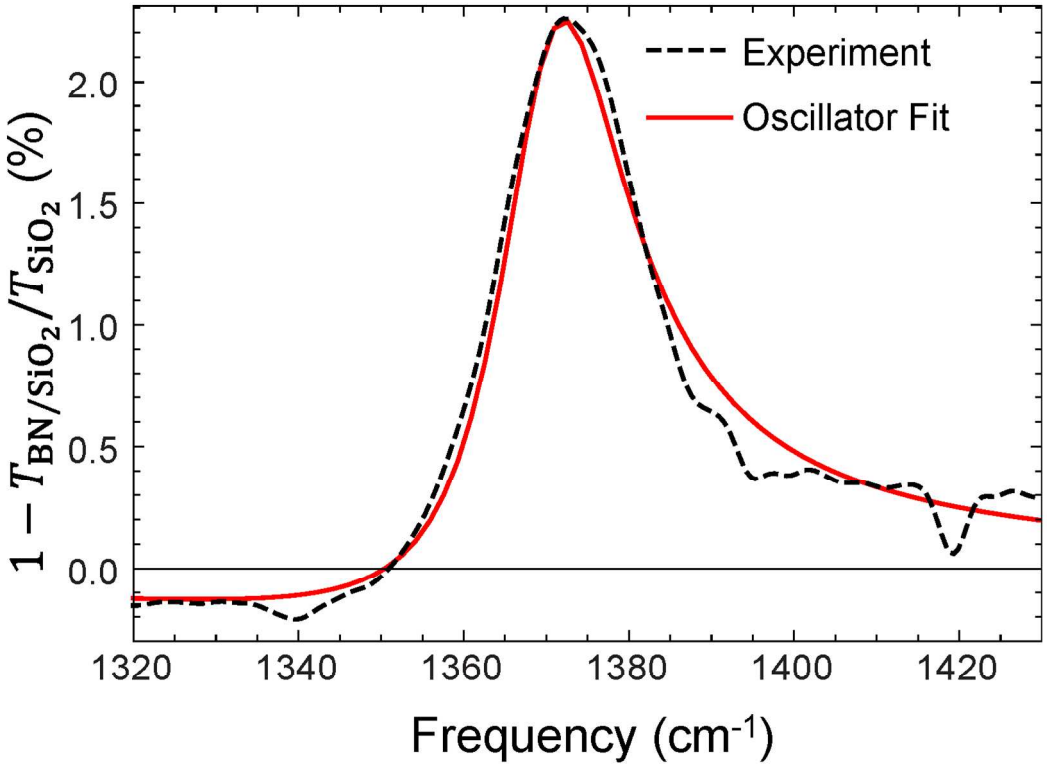

Figure S1: **h-BN optical phonon extinction spectra.** Extinction spectra of h-BN/SiO_2/Si sample normalized by transmission through bare SiO_2/Si sample. Absorption peak at 1370cm^{-1} is due to the h-BN in plane optical phonon oscillation. The measured data (black dashed) can be fitted well with theoretical spectra assuming an oscillator model for h-BN dielectric function (red).

2. Carrier Density Dependence of Graphene/h-BN plasmon and SPPP modes

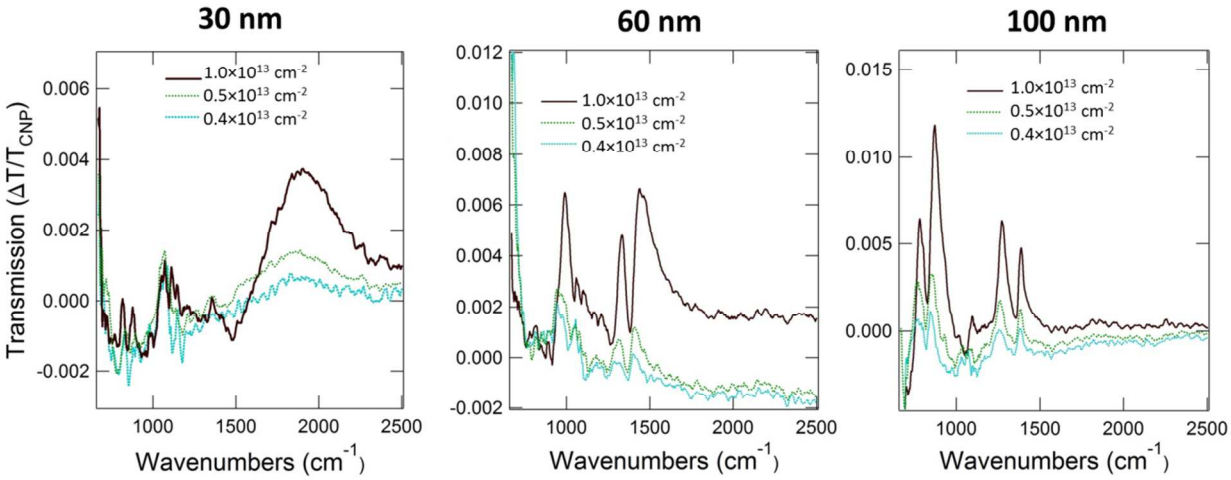

Figure S2: **Experimental dependence of transmission modulation on carrier density.** Measured transmission modulation spectrum at various carrier densities for 30 (left), 60 (middle), and 100nm (right) graphene nanoresonators. In all cases, the peaks are blue shifted and becomes stronger with increasing doping concentration.

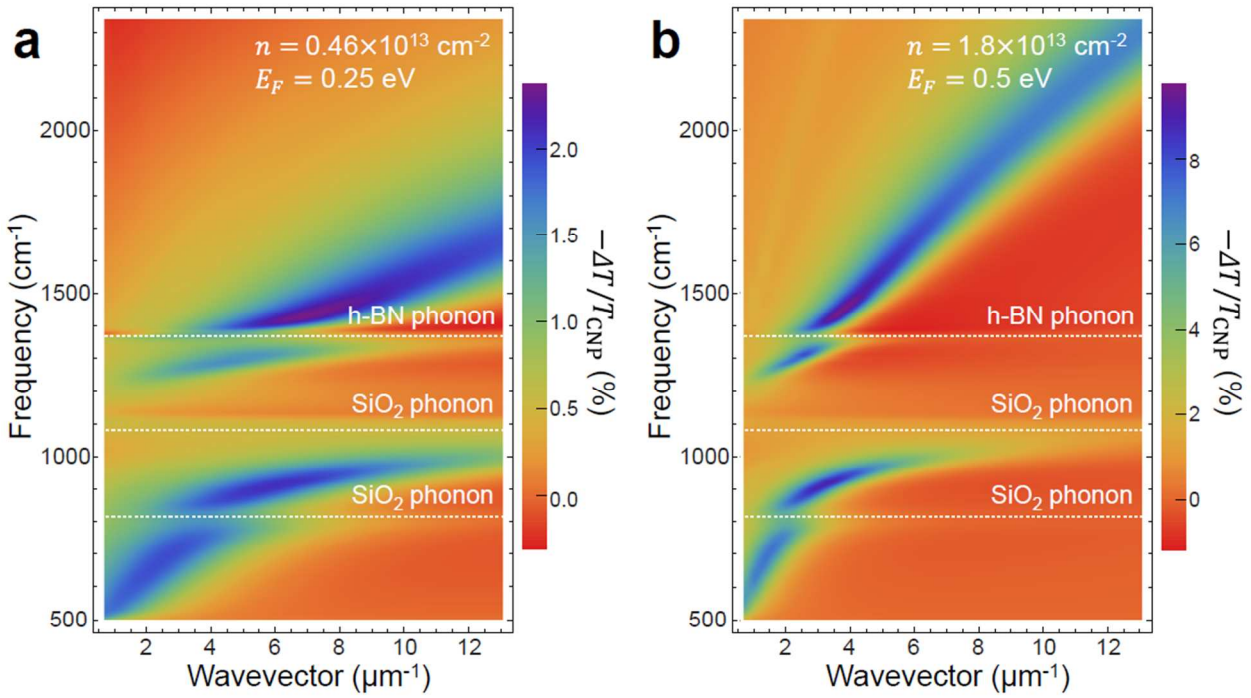

Figure S3: **Carrier density dependence of plasmons in graphene/h-BN.** Calculated change in transmission for graphene/monolayer h-BN nanoresonators of varying width at low (n = 0.46×10^{13} cm^{-2}) and (b) high (n = 1.8×10^{13} cm^{-2}) carrier densities. The wavevector is determined by considering the ribbon width, W, as well as the phase of the plasmon reflecting off the graphene ribbon edge.

3. Characterization of h-BN in areas exposed to 100keV e-beam and O_2 plasma

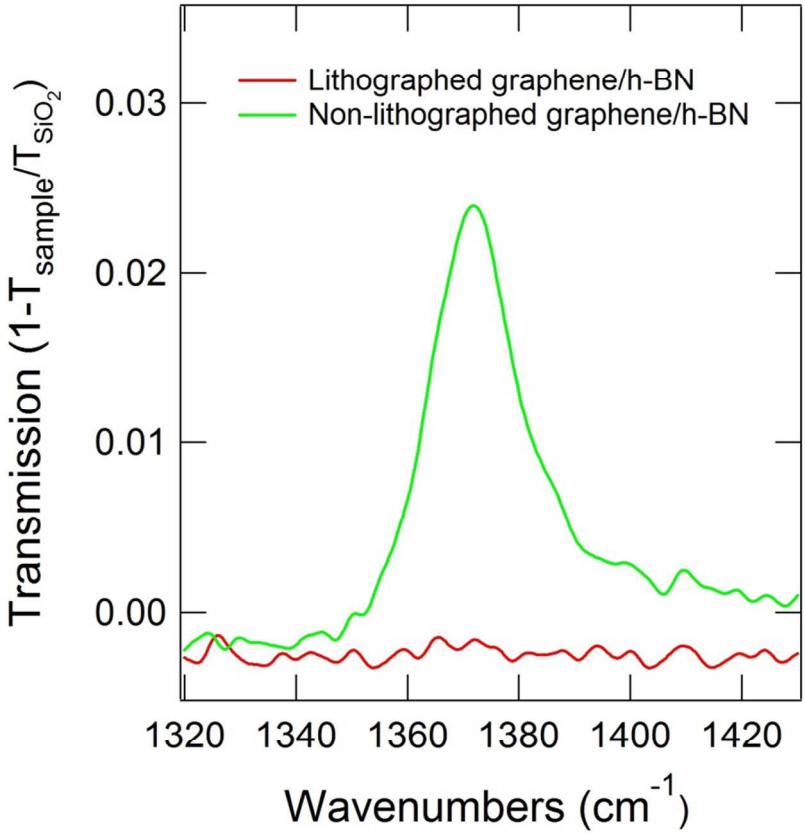

Figure S4: **Optical characterization of graphene/h-BN areas exposed to lithography process.** Measured transmission modulation spectrum from a continuous 50x50μm^2 region of graphene/h-BN exposed to the 100keV in PMMA electron beam patterning process in PMMA, followed by the O_2 plasma etch (red line). For comparison, the transmission spectrum from an untouched region of graphene/h-BN is included (green line). These spectra reveal that the optical absorption peak at 1370cm^{-1} due to the in-plane optical phonon of h-BN is lost in the lithography process, indicating that the h-BN sheet has been degraded.

4. Determination of carrier density of graphene sheet

Interband transitions occur in graphene when the incident photon energy is higher than two times of the Fermi level (E_F) of the graphene, and thus it is possible to estimate the Fermi energy from the transmission modulation due to the onset of interband transition.[6] As a reference signal, we first took a near infrared transmission spectrum at the charge neutral point (CNP). Here the charge neutral condition was achieved by applying the gate voltage (V_{CNP} = 165V) which gave a maximum in the resistance as shown in Fig. S5. The near-IR transmission spectra at various gate voltage values (V_G) were then taken, and normalized with respect to the reference spectrum in order to see the difference. The resulting transmission modulation spectra of an area patterned with 80nm nanoresonators at V_G = −90V and V_G = 0V (background doping) are presented in Fig.S6, and they both exhibit a downward slope which is originated from the onset of the interband transition. We observe that the $2E_F$ interband onset is considerably wider than the theoretical estimate for thermal broadening of $2E_F$ at room temperature, which is consistent with the observation by Li et al.[6] In order to determine the carrier densities at each V_G values, we obtained the theoretical transmission spectra which give the best fit to the measured data by using both the Fermi level position and broadening as fitting parameters. As a result, the carrier densities are determined to be $n = 1.0\times10^{13}$ cm^{-2} (hole doped) for the highest carrier density used in this experiment, and $n = 0.4\times10^{13}$ cm^{-2} (hole doped) as the background doping. The theoretical spectra were calculated by numerically solving classical electromagnetic equations using finite element method.[1, 7] The background doping observed in our samples has been shown previously to be mainly caused by the FeCl etchant that is used to remove the copper foil from the as-grown CVD graphene,[7] although atmospheric impurities, and charge traps in the substrate can also play a role.[8, 9] Interband transition measurements and E_F fittings performed on bare graphene areas

showed a similar gate vs. carrier density dependence to the patterned graphene areas, as was also observed in previous works.[7]

We note that the carrier density we extract by monitoring the interband transitions is lower that what would be obtained from a simple parallel plate capacitance calculation for our device.[10, 11] We attribute this to two possible effects. First, our measurements were performed under nitrogen purged conditions, where atmospheric impurities were still, inevitably present. These impurities cause hysteresis in our gate-dependent resistance curves, and have been shown to change the gate voltage vs. carrier density relationship in graphene devices.[12-14] Second, it has been shown that impurities on graphene that contain states near the Dirac point can be charged and discharged as the graphene Fermi level is varied via the applied gate bias.[15, 16] This charging and discharging process cause the background doping to have a gate dependence (as impurities are turned 'on' and 'off') , and thus alter the expected gate voltage vs. carrier density dependence. Such impurity states could be intrinsic to the CVD h-BN sheet, or could be introduced during the fabrication process by either PMMA residue on top of the graphene, or impurities trapped between the graphene and h-BN sheets. For these reasons, we feel that fitting the high energy transmission spectrum, where the interband transitions occur, is the most direct and accurate way to determine the graphene nanoresonator carrier density.

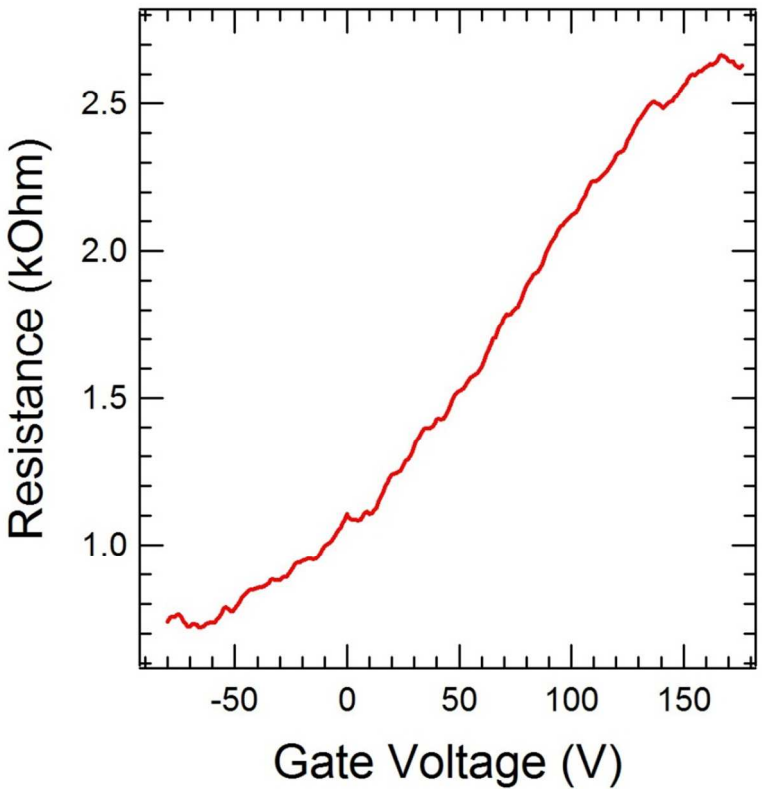

Figure S5: **Resistance vs. applied gate voltage for graphene/h-BN device.** Measured two-probe resistance value of the graphene sheet on monolayer h-BN. The maximum in resistance occurs at 165V, corresponding to the gate voltage that removes all free carrier from the graphene sheet and aligns the Fermi level with the Dirac point.

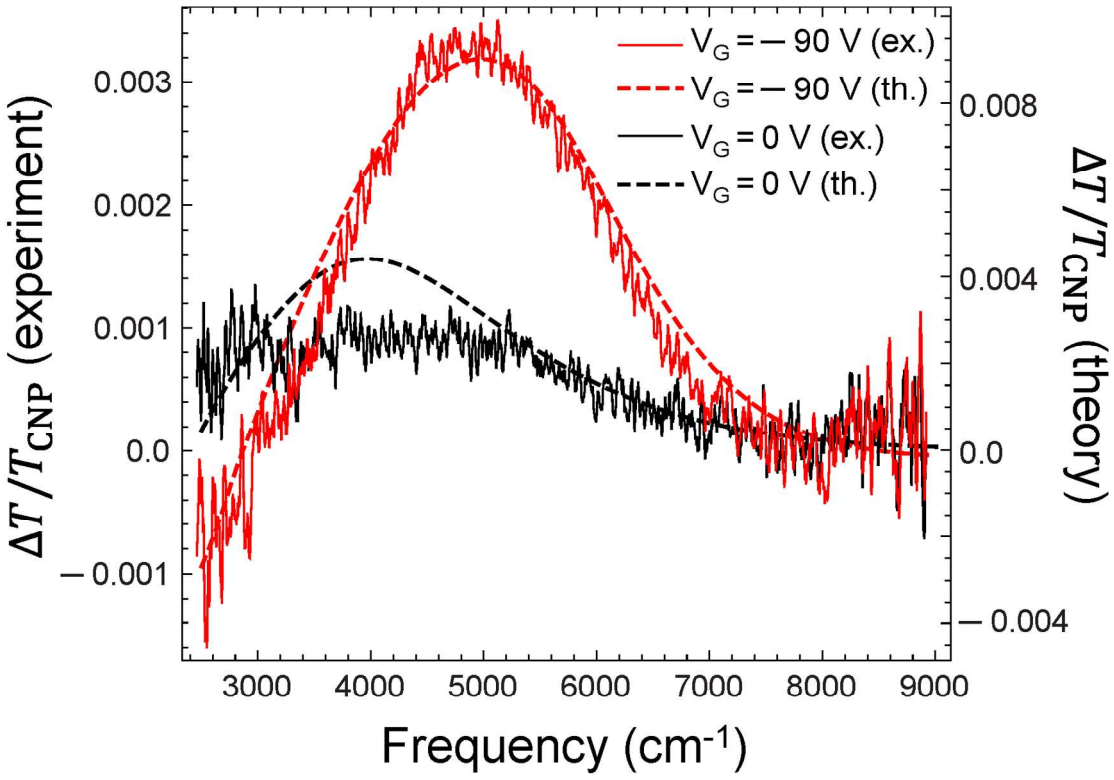

Figure S6: **Change in transmission due to blocking of interband transitions.** (Solid lines) Normalized near IR experimental spectra taken with $V_G = -90$V ($\Delta V_G = -255$V) and $V_G = 0$V ($\Delta V_G = -165$V) from an area of the graphene/h-BN sample patterned with 80nm nanoresonators. (Dashed lines) Fitted theoretical change in transmission giving $n = 1.0\times10^{13}$ cm^{-2} for $V_{gG} = -90$V and $n = 0.4\times10^{13}$ cm^{-2} for $V_G = 0$V (intrinsic doping).

References

1. Falkovsky, L. A.; Varlamov, A. A. *Eur. Phys. J. B* **2007,** 56, (4), 281-284.
2. Jablan, M.; Buljan, H.; Soljacic, M. *Phys Rev B* **2009,** 80, (24), 245435.
3. Park, C.-H.; Giustino, F.; Cohen, M. L.; Louie, S. G. *Physical Review Letters* **2007,** 99, (8), 086804.
4. Geick, R.; Perry, C. H.; Rupprecht, G. *Physical Review* **1966,** 146, (2), 543-547.
5. Palik, E. D., Handbook of Optical Constants of Solids. Elsevier.

6. Li, Z. Q.; Henriksen, E. A.; Jiang, Z.; Hao, Z.; Martin, M. C.; Kim, P.; Stormer, H. L.; Basov, D. N. *Nat Phys* **2008,** 4, (7), 532-535.

7. Brar, V. W.; Jang, M. S.; Sherrott, M.; Lopez, J. J.; Atwater, H. A. *Nano Lett* **2013,** 13, (6), 2541-2547.

8. Martin, J.; Akerman, N.; Ulbricht, G.; Lohmann, T.; Smet, J. H.; Von Klitzing, K.; Yacoby, A. *Nat Phys* **2008,** 4, (2), 144-148.

9. Zhang, Y. B.; Brar, V. W.; Girit, C.; Zettl, A.; Crommie, M. F. *Nat Phys* **2009,** 5, (10), 722-726.

10. Novoselov, K. S.; Geim, A. K.; Morozov, S. V.; Jiang, D.; Katsnelson, M. I.; Grigorieva, I. V.; Dubonos, S. V.; Firsov, A. A. *Nature* **2005,** 438, (7065), 197-200.

11. Novoselov, K. S.; Geim, A. K.; Morozov, S. V.; Jiang, D.; Zhang, Y.; Dubonos, S. V.; Grigorieva, I. V.; Firsov, A. A. *Science* **2004,** 306, (5696), 666.

12. Levesque, P. L.; Sabri, S. S.; Aguirre, C. M.; Guillemette, J.; Siaj, M.; Desjardins, P.; Szkopek, T.; Martel, R. *Nano Letters* **2010,** 11, (1), 132-137.

13. Ryu, S.; Liu, L.; Berciaud, S.; Yu, Y.-J.; Liu, H.; Kim, P.; Flynn, G. W.; Brus, L. E. *Nano Letters* **2010,** 10, (12), 4944-4951.

14. Wang, H.; Wu, Y.; Cong, C.; Shang, J.; Yu, T. *ACS Nano* **2010,** 4, (12), 7221-7228.

15. Brar, V. W.; Decker, R.; Solowan, H. M.; Wang, Y.; Maserati, L.; Chan, K. T.; Lee, H.; Girit, C. O.; Zettl, A.; Louie, S. G.; Cohen, M. L.; Crommie, M. F. *Nat Phys* **2011,** 7, (1), 43-47.

16. Pi, K.; McCreary, K. M.; Bao, W.; Han, W.; Chiang, Y. F.; Li, Y.; Tsai, S. W.; Lau, C. N.; Kawakami, R. K. *Physical Review B* **2009,** 80, (7), 075406.